T.T. Belete, M.C.M. van de Sanden, M.A. Gleeson
Sustainable Materials and Technologies 25 (2020) e00163
https://doi.org/10.1016/j.susmat.2020.e00163

Performance of transition metal-doped $CaCO_3$ during cyclic CO_2 capture-and-release in low-pressure H_2O vapour and H_2O plasma.

T.T. Belete, M.C.M van de Sanden, and M.A. Gleeson.

DIFFER - Dutch Institute for Fundamental Energy Research,
De Zaale 20,5612 AJ Eindhoven, the Netherlands.

Keywords: Calcium carbonate; Transition metal doping; Calcium looping cycle; Calcination; Carbonation; CO_2 capture; Water plasma.

Abstract

The effects of transition metal doping of calcium carbonate on the subsequent performance of the material during CO_2 release and recapture have been evaluated for calcination under low-pressure (~0.1 mbar) water vapour and water plasma conditions. The initial samples were prepared by precipitation method from analytical grade carbonate, calcium and transition metal (Fe, Co, Zn, Cu and Ni) containing precursors. The release-recapture properties of the sorbents were monitored over five cycles involving calcination at 1200 K and carbonation at 825 K. The most noteworthy effects were observed for the Zn-doped samples, which exhibited rapid CO_2 recapture.

Calcination in H_2O plasma was tested to evaluate the potential for *in-situ* material processing as a means to counteract material degradation. The impact of plasma exposure during calcination on the looping performance was mixed and dependent on the specific sample composition. The performance of the Zn-doped $CaCO_3$ was consistently improved by plasma calcination, yielding high uptake and better retention of carrying capacity over the five cycles.

All samples exhibited a deterioration in carrying capacity over repeated cycles The Zn-doped samples also performed best in this respect (least loss of carrying capacity).The beneficial effects of Zn-doping were dependent on the Zn-content of the precursor solutions used for material synthesis.

Introduction

Carbon dioxide emissions associated with the use of fossil fuels for energy generation, transportation, and industrial production are of pressing environmental concern in light of their contribution to driving global climate change [1], [2]. Increasing demand for energy associated with rapid regional development and growing world population means that fossil fuels may continue to be used as a significant source of energy over the coming decades. Several options, such as CO_2 capture and storage [3]–[5], CO_2 utilization [6]–[8], CO_2 mineralization [9], [10], and expanded usage of low carbon fuels [11], are proposed to mitigate emissions. One of the most feasible means to realise short- to mid-term mitigation is carbon capture from flue gases and other industrial sources. Captured CO_2 can be sequestered or used as raw material for the production of synthetic fuels or value-added chemicals.

The high-temperature Calcium Looping (CaL) cycle, which is based on cyclic CaO-$CaCO_3$ calcination/carbonation reactions, is a promising candidate for CO_2 capture from industrial sources. CaL is a relatively mature technology capable of implementation on a large scale. A schematic of a CaL cycle is presented in Figure 1. In CaL a major portion of the CO_2 in flue gas that enters the carbonator reacts with calcium oxide (CaO) at ~650 °C, producing calcium carbonate ($CaCO_3$) while other, environmentally benign, gases are released into the atmosphere.

The carbonated sorbent is regenerated in a calciner and reused in the subsequent capture step (Route #1 in Figure 1), ideally producing a concentrated (up to 95 %) stream of CO_2 [12]. Calcination

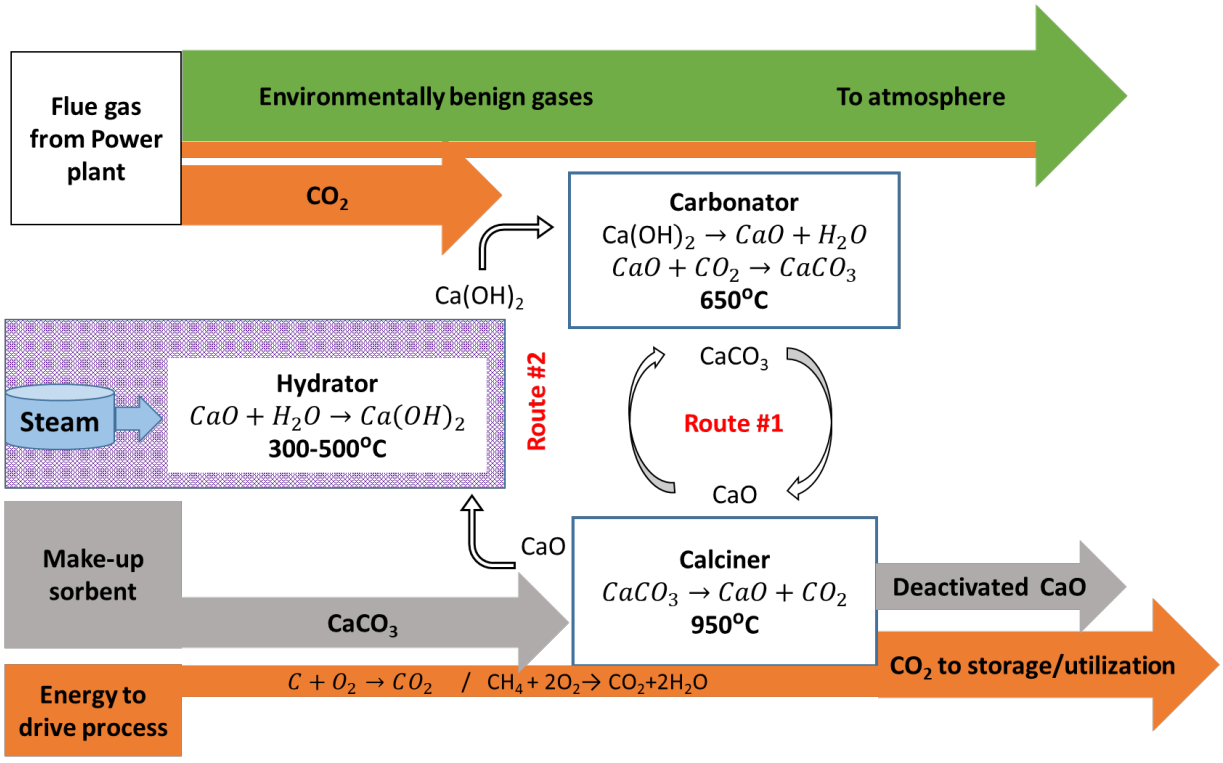

Figure 1: Schematic representation of the calcium looping cycle with oxy-combustion (Route #1), and with the addition of a hydrator for sorbent reactivation (Route #2).

is an endothermic process that is typically performed at ~950 °C and atmospheric pressure. The energy required to drive the process can be delivered to the system through oxy-combustion of coal [12]–[14] or carbon-containing fuel [15], [16] that simultaneously yields a pure CO_2 stream under which calcination is performed. The combined stream of CO_2 from calcination of $CaCO_3$ and oxy-combustion can be compressed and transported for storage or utilized as a carbon source.

The sorbent material should, ideally, go through multiple cycles of capture and release without degradation. However, the capture capacity of CaO typically deteriorates over multiple cycles as a result of temperature-induced material sintering, which decreases CO_2 uptake by reducing surface area and inducing pore closure [17]–[19]. As a consequence, degraded material should be periodically removed and fresh sorbent introduced in order to compensate for deactivation. Various sorbent reactivation methods such as steam/water hydration, thermal pre-treatment [20], [21], production of synthetic sorbents [22], and doping [23], [24] have been studied as part of efforts to counter-act the sintering process.

Promising results have been obtained by steam/water hydration of CaO [19], [25]–[27] and by steam reactivation of spent sorbent [19]. Addition of such processes to the cycle is indicated in Figure 1 (Route #2) in the form of a third reaction vessel (Hydrator), operating at a lower temperature/higher pressure, that is used to regenerate sorbents. In this case, the cycle is comprised of three steps: hydration of CaO, carbonation of $Ca(OH)_2$, and calcination of $CaCO_3$ as represented by Eq. (1-3) respectively.

$$CaO(s) + H_2O(g) \leftrightharpoons Ca(OH)_2(s) \quad \Delta H_{f298K} = -109\ kJ/mol \tag{1}$$

$$Ca(OH)_2(s) + CO_2(g) \leftrightharpoons CaCO_3(s) + H_2O(g) \quad \Delta H_{f298K} = -69.0\ kJ/mol \tag{2}$$

$$CaCO_3(s) \leftrightharpoons CaO(s) + CO_2(g) \quad \Delta H_{f298K} = 178\ kJ/mol \tag{3}$$

Complete hydration of CaO (molar volume of 17 $cm^3.mol^{-1}$) leads to expansion upon the formation of $Ca(OH)_2$ (molar volume of 33 $cm^3.\ mol^{-1}$) followed by the formation of a network of pores upon dehydration which improves regeneration of the sorbent [22]. However, hydration of CaO is also observed to become less effective with increasing number of cycles [26], [28].

A number of researchers have doped calcium-based sorbents (Si, Ti, Cr, Co, Zr, and Ce [29], La, Y, Hf, W, and Al [30], salts of KCl and K_2CO_3 [24], and salts of NaCl and Na_2CO_3 [31]) in efforts to develop materials with good mechanical strength, resistance to sintering and improved CO_2 capture performance. The objective of the current work is to investigate the CaL performance of transitional metal (TM) doped sorbents. Our previous report [32] on the effects of transition metal dopants on the calcination of $CaCO_3$ showed that TM-doping resulted in a reduction in the calcination temperature of the as-prepared samples relative to Pure $CaCO_3$. This paper focusses on evaluating the extent to which the performance of the different samples is affected over repeated cycling with calcination in either low-pressure H_2O vapour or H_2O plasma. While the low-pressure experimental conditions used are not representative of application conditions, the self-consistent procedures used allow valid cross-comparisons regarding the relative performance of

the samples to be made in order to evaluate the impact of doping and calcination environment on the performance.

As noted above, the presence of H_2O vapour can be anticipated to enhance calcination [33]. The motivation to compare with calcination in H_2O plasma is linked to several potential benefits. Plasma produces excited/activated H_2O molecules, which may facilitate decomposition of $CaCO_3$ [34]. Calcination in plasma introduces conversion of the captured CO_2 into CO during the release. H_2 produced directly in H_2O plasma may also assist in this process. As first reported in [35], [36], thermal decomposition of TM-doped $CaCO_3$ in H_2 can produce CO and even CH_4. Detailed consideration of these plasma-chemical conversion effects are outside the scope of the current work and will be addressed in a future report. This report concentrates primarily on the impact of TM-doping and plasma exposure on the cyclical performance of capture and release of CO_2 by the samples in order to determine if the physical effects of plasma on the sorbent can assist in counteracting material degradation through sintering.

Experimental

Sample preparation

All carbonate samples were prepared by precipitation method from analytical grade commercial precursors based on $CaCl_2•2H_2O$, Na_2CO_3, $CoCl_2•6H_2O$, $FeCl_3•6H_2O$, $NiCl_2•6H_2O$, $CuCl_2•2H_2O$, and $ZnCl_2$ (Sigma-Aldrich, Germany). Pure $CaCO_3$ was prepared by mixing of 0.8 M $CaCl_2$ solution and 0.8 M Na_2CO_3 solution at room temperature (20-23°C). Two sets of samples doped with Co, Ni, and Fe were synthesized based on addition of the relevant TM chloride amounting to 1.0 wt.% and 2.5 wt.% of the corresponding $CaCl_2•2H_2O$ component to the initial chloride solution prior to mixing with the carbonate solution. Table 1 gives an overview of precursor solution compositions. Precipitation was initiated by pouring the chloride-containing solution into a beaker containing the continuously-stirred carbonate solution. The inception of precipitation was immediate in all cases. The mixed solution was stirred for 10-15 minutes to stimulated complete precipitation.

Table 1: Molar concentrations (M) and volumes of deionized-water (ml) of the precursor solutions used for Pure, Fe-, Co-, and Ni-doped sample synthesis. The relevant calcium and TM chloride solutions were first mixed and the resultant solution was added to the carbonate solution as described in the text.

		Chloride solutions		Carbonate solutions	TM:Ca
TM (wt.%)	**Sample**	*$CaCl_2.2H_2O$*	*TM chloride*	*Na_2CO_3*	*molar ratio*
0	Pure	0.80M [250ml]	-	0.80M [250ml]	-
1.0	Fe-doped	1.24M [200ml]	$FeCl_3•6H_2O$ - 0.054M [25ml]	1.25M [200ml]	0.0054
	Co-doped	1.24M [200ml]	$CoCl_2•6H_2O$ - 0.062M [25ml]	1.25M [200ml]	0.0062
	Ni-doped	1.24M [200ml]	$NiCl_2•6H_2O$ - 0.062M [25ml]	1.25M [200ml]	0.0062
2.5	Fe-doped	0.81M [150ml]	$FeCl_3•6H_2O$ - 0.080M [25ml]	0.83M [150ml]	0.0140
	Co-doped	0.80M [150ml]	$CoCl_2•6H_2O$ - 0.080M [25ml]	0.83M [150ml]	0.0160
	Ni-doped	1.22M [200ml]	$NiCl_2•6H_2O$ - 0.080M [50ml]	1.25M [200ml]	0.0150

Attempts to precipitate solids in a similar manner from precursor solutions containing Cu- and Zn-dopants were unsuccessful due to the tendency of these ions to inhibit calcite growth in the solution [37]. Consequently, Cu- and Zn-doped $CaCO_3$ samples were prepared by mixing of separately prepared TM carbonate and calcium carbonate precipitation solutions. The molar

concentrations and volumes used to prepare the 1.0 wt.% and 2.5 wt.% doped samples are listed in Table 2. A 5.0 wt.% Zn sample was also prepared in a similar manner, as indicated in Table 2. Once mixed, the individual carbonate solutions were quickly (within 10 s) combined to minimize precipitation of the pure carbonate form. The combined carbonate solutions were stirred for 30 minutes to stimulate complete precipitation.

Table 2: Molar concentrations (M) and volumes of deionized-water (ml) of the precursor solutions used for Cu-, and Zn-doped sample synthesis. The calcium carbonate and TM carbonate solutions were prepared separately and then quickly mixed as described in the text.

		Calcium carbonate solutions		TM carbonate solutions		TM:Ca
TM (wt.%)	Sample	*$CaCl_2.2H_2O$*	*Na_2CO_3*	*TM chloride*	*Na_2CO_3*	*molar ratio*
1.0	Cu-doped	1.24M [200ml]	1.23M [200ml]	$CuCl_2$•$2H_2O$ - 0.086M [25ml]	0.14M [25ml]	0.0087
	Zn-doped	1.24M [200ml]	1.23M [200ml]	$ZnCl_2$ - 0.11M [25ml]	0.14M [25ml]	0.0108
2.5	Cu-doped	0.73M [100ml]	0.72M [100ml]	$CuCl_2$•$2H_2O$ - 0.075M [25ml]	0.10 M [25ml]	0.0220
	Zn-doped	0.97M [150ml]	0.96M [150ml]	$ZnCl_2$ - 0.16M [25ml]	0.21M [25ml]	0.0270
5.0	Zn-doped	0.71M [200ml]	0.69M [200ml]	$ZnCl_2$ – 0.32M [25ml]	0.41M [25ml]	0.0560

Calcination-Carbonation cycling

The cyclic calcination-carbonation performance of the samples was tested in the same experimental setup that was used in the preceding study [32]. It consists of three sections as depicted in Figure 2. The first section contained the sample (~10^{-3} mbar base pressure; working pressures up to ~10 mbar). The sample is held above the heating element of a commercial resistive heating stage (UHV-Design) in a circular tray made of Titanium-Zirconium-Molybdenum (TZM) alloy. The process temperature is monitored with a K-type thermocouple mounted in a fixed position near the sample tray. Heating is controlled by a custom-built controller with a PID feedback system.

The second section has a base pressure of ~10^{-8} mbar. It is separated from the sample section by a 200 µm aperture and could be fully isolated by means of a pneumatic valve. The third section (~10^{-9} mbar base pressure) is separated from the second section by a 2 mm aperture. It contains a Quadrupole Mass Spectrometer (QMS; Hiden Analytical HALO). When the pneumatic valve is open,

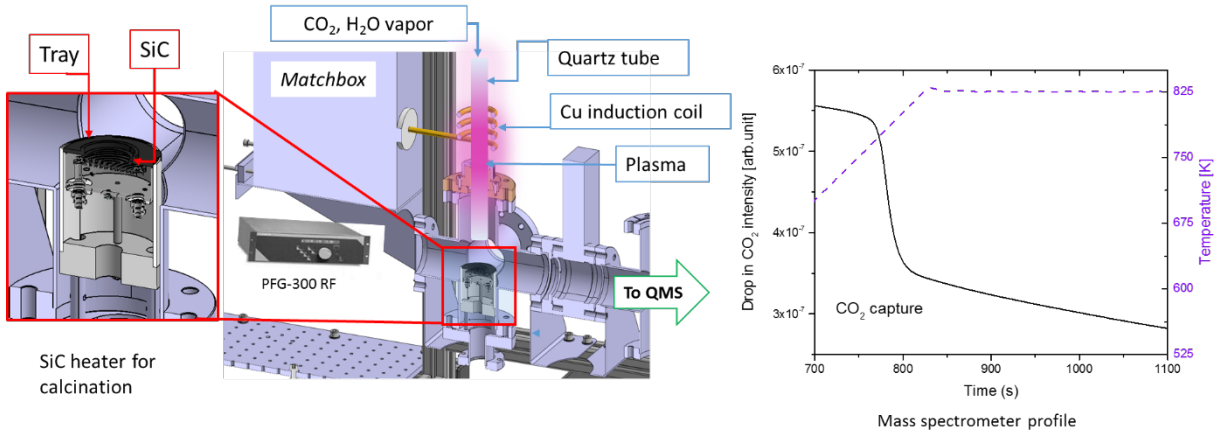

Figure 2: Overview of the experimental setup used for CO_2 capture and release. During release H_2O is introduced from the top (plasma is ignited for release in plasma). During capture CO_2 is introduced from the top. The mass spectrometer profile on the right illustrates a measured CO_2 intensity decrease as a result of temperature-induced CO_2 capture by a Zn-doped sample (details later in the text).

the ionizer of the QMS is in direct line-of-sight of the heating section via the two apertures. The QMS is used to monitor the time-dependent evolution of selected gases (both introduced and evolved from the sample) during calcination-carbonation cycles.

Typically ~150 ± 1.0 mg of the synthesized sample was used for testing. Gases were introduced into the first section via the quartz tube. Water vapour was introduced from a stainless-steel reservoir via a needle valve. The deionized water in this reservoir was degassed by means of several freeze-pump-thaw cycles before use. To maintain a constant pressure of H_2O vapour, the water reservoir was maintained at 26°C using a water bath (PolyScience). Plasma was ignited using a radiofrequency power generator (PFG-300 RF, Hüttinger Elektronik GmbH + Co. KG, Germany) by means of inductive coupling from a water-cooled hollow copper coil surrounding a quartz tube of 30 cm in length and 2 cm in diameter. The generator is connected to a matching box through the coaxial cable of 50 Ω internal impedance. The matching network is connected directly to the coil.

Calcination was performed under ~0.1 mbar H_2O vapour or H_2O plasma by ramping the sample temperature linearly to 1200 K at a rate of 1 K/s followed by holding at that temperature for 180 s. The working pressure was established and, where relevant, the plasma was ignited prior to the start of the temperature ramp. An input power of 100 W was used in case of calcination under H_2O plasma. Once the thermal cycle was completed and the sample began to cool, the plasma was extinguished (where applicable) and the water flow was stopped.

Carbonation of the calcined sorbents was performed by filling the first section of the vacuum vessel with CO_2 to a pressure of ~5 mbar without active pumping ("static" pressure). In this configuration, there is a gradual decrease in the CO_2 level due to slow pumping via the second section through the first aperture. Once the CO_2 was introduced, the temperature was ramped to 825 K at a rate of 1 K/s and then held at this temperature for 600 s. As the carbonation process is accelerated at elevated temperature, the sample begins to act as a "pump" and the CO_2 pressure in the chamber is observed to decrease at a faster rate (see the illustrative plot in Figure 2). The selection of 825 K as the plateau temperature was based on evaluation of the recapture behaviour of Pure $CaCO_3$ samples as a function of temperature. If the temperature was significantly higher than this value, the sample would begin to re-release some of the CO_2 already captured during the carbonation. Once the carbonation thermal cycle was completed, residual CO_2 was pumped away and the sample was allowed to cool in preparation for the subsequent calcination phase. Five consecutive calcination-carbonation cycles of the (doped-)$CaCO_3$ sorbents were performed. The sample temperature was allowed to drop below 500 K after both calcination and carbonation before the next phase in the cycle was initiated.

As-prepared and calcined samples were characterized by means of X-ray diffraction (XRD - D8 advance Eco, Bruker, Karlsruhe, Germany) using a Cu-Kα radiation source (λ=1.5406 Å) at 40 keV and 25 mA. Diffraction patterns were collected in Bragg-Brentano θ/2θ geometry over the range of 20°≤ 2θ ≤ 60° with a step of 0.01°. Qualitative identification of phases was performed using Match! software (Crystal Impact, Bonn, Germany) and quantitative analysis by running Rietveld refinements from within Match!, with the actual calculations being automatically performed using

the program FullProf [38] in the background. Scanning electron microscopy (Phenom Pharos Desktop SEM, Thermo Scientific) was performed on samples with 15 kV accelerating voltage in backscattered mode.

Results and discussion

a. Cyclic capture-release in 0.1 mbar H_2O vapour

The first step in the evaluation of the materials was calcination of the as-prepared Pure and TM-doped $CaCO_3$ in H_2O vapour at 1200 K. XRD measurements confirm that these samples are fully carbonate. Consequently, they are representative of a fully-loaded material. Figure 3 shows CO_2 traces that were measured during the initial calcination. Each measured trace has been divided by its own integrated area. Thus, the plotted values represent the instantaneous fractional release based on the assumption that the sample is fully depleted at the end of the calcination cycle. This is an approximation since the elevated CO_2 level at t=1380s shows that complete calcination has not yet occurred. The differences in release time (temperature) evident in Figure 3 are primarily the result of the presence of TM-dopants, although the presence of H_2O vapour also has an influence (see Reference [32] for details).

After the initial calcination, each sample was kept in place for five successive carbonation-calcination cycles. Figure 4 shows the measured CO_2 response during the carbonation portions of these five cycles. “Capture 1” refers to carbonation directly after the calcination of the as-prepared sample. Uptake of CO_2 by the samples is evident from changes in the rate at which the signal decreases. As the samples become saturated, the rate of decrease drops and the signal reverts to the characteristic decay rate produced by the aperture pumping.

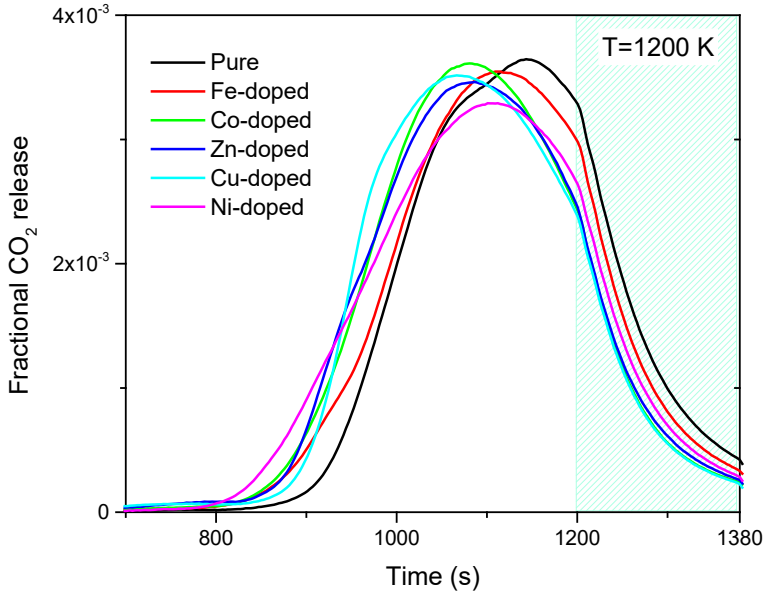

Figure 3: Fractional CO_2 release from as-prepared Pure and 2.5 wt.% TM-doped $CaCO_3$ during calcination in ~0.1 mbar H_2O vapour. The time axis has been shifted such that the time values (t≤1200 s) are equivalent to the temperature values during the ramping phase. The shaded region indicates the temperature plateau region (T=1200 K).

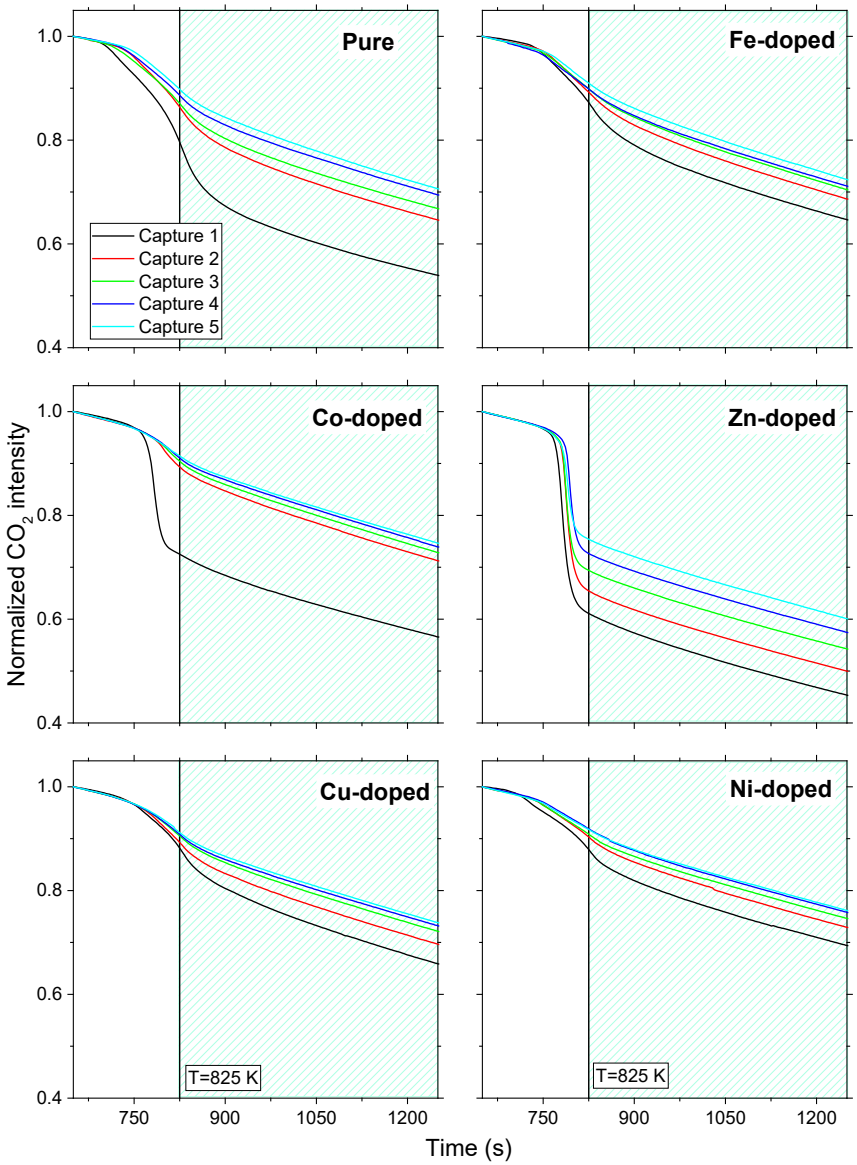

Figure 4: Normalized CO_2 intensity during the capture portion of five successive capture-release cycles for Pure and 2.5 wt.% TM-doped samples. The trace legend applies to all panels. The time axes have been shifted such that the time values are equivalent to the temperature values during the ramping phase (t≤825 s). The shaded regions indicate the temperature plateau region (T=825 K). Traces have been normalized to the intensity value at T=670 K.

To better illustrate the characteristics and evolution of CO_2 uptake by the different samples, the CO_2 traces measured during capture were differentiated to yield a representation of the CO_2 capture rate. The effect of pumping via the aperture is still included in this data, resulting in an offset of the differentiated curves from zero even when there is no appreciable uptake by the sample. Figure 5 shows differentiated curves obtained for recapture by the Pure sample (top panel) and by the 1.0 wt.% (left-hand column panels) and 2.5 wt.% (right-hand column panels) TM-doped samples. The Y-axes of all main panels are identical, with the range being determined by the sorbent that exhibits the fastest CO_2 uptake, namely the 2.5 wt.% Zn-doped sample. The insets on individual panels provide an expanded view of the uptake region in cases where the traces are not

clearly visible on the main panel. The solid vertical line on each panel and inset indicates the point at which the 825 K plateau temperature is attained.

Clearly, the different sorbents have significantly different recapture characteristics. All samples begin to capture CO_2 at a significant rate during the ramping phase. The most notable feature of

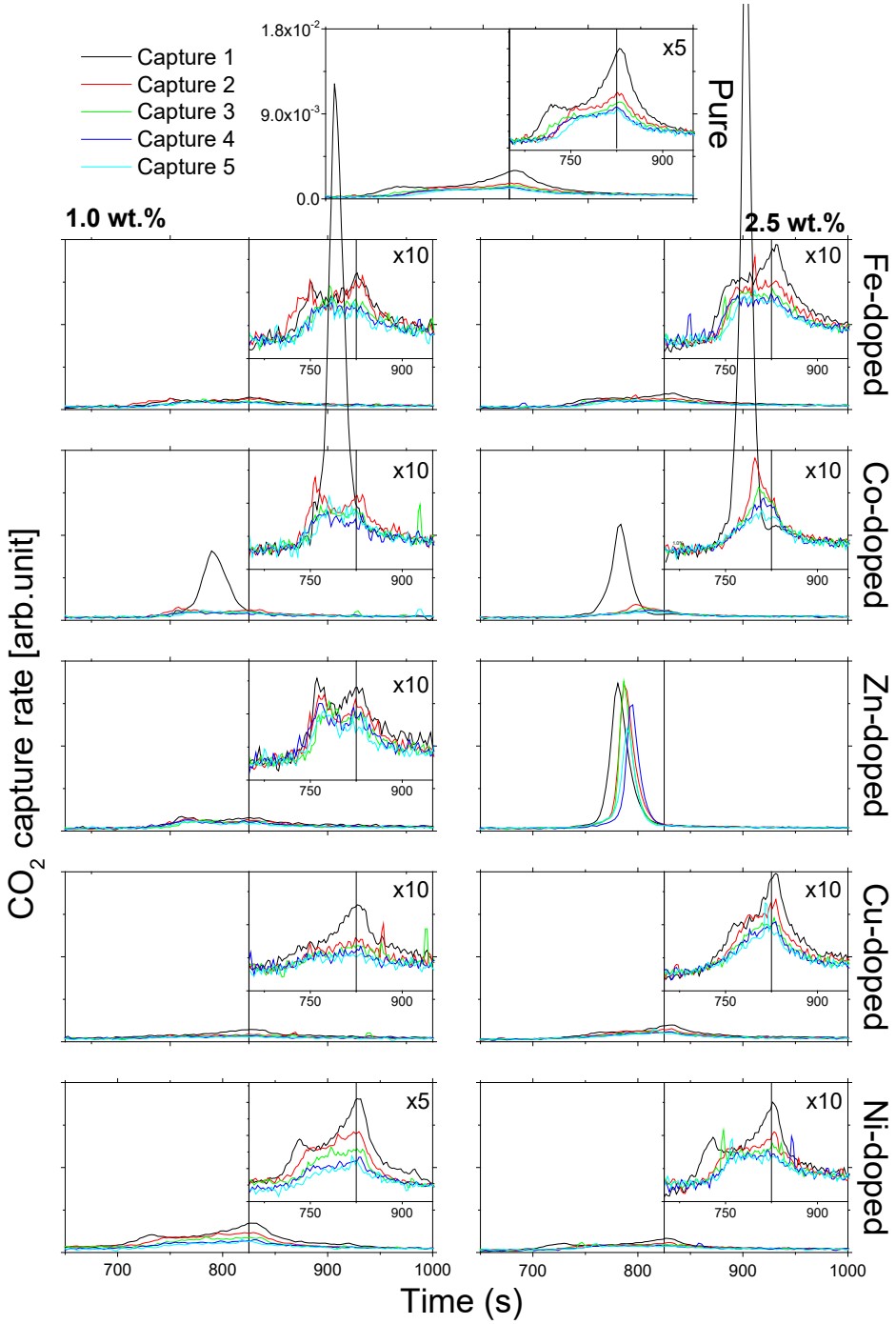

Figure 5: CO_2 recapture rates of Pure (top panel), 1.0 wt.% (left column) and 2.5 wt.% (right column) TM-doped $CaCO_3$ samples after calcination in ~0.1 mbar H_2O vapour. The trace legend applies to all panels. Panel insets show expanded views of the main panel data. The vertical lines indicate the transition from the 1 K/s temperature ramp to the T=825 K temperature plateau phase.

Figures 4 and 5 is the very rapid uptake of CO_2 by the 2.5 wt.% Zn-doped sample, which persists over all five cycles. Recapture by this sample is essentially completed before the plateau temperature is attained, although the uptake does exhibit a shift toward higher temperature with successive cycles. The 1.0 wt.% Zn-doped sample does not exhibit a similar rapid uptake, suggesting that the effect has a significant concentration dependence (more details later). Both the 1.0 wt.% and 2.5 wt.% Co-doped samples exhibit rapid uptake during the first capture step, but the effect does not recur during subsequent cycles. The other samples show a more gradual (extended) uptake as a function of time/temperature and continue to capture CO_2 for some time after the temperature has stabilized. These samples generally exhibit a double structure in the uptake profile, with the capture rate first peaking (or plateauing) during the ramping phase before subsequently increasing again at a higher temperature. The second peak in the capture rate generally coincides with the attainment of the plateau temperature. This shape can be rationalized in terms of the model of rapid formation of a closed surface carbonate layer, followed by slower, diffusion-limited, uptake by the material bulk [39], [40]. In contrast, the single-peak uptake curves of Zn and Co indicate more uniform carbonate formation, suggesting that these dopants are inhibiting the formation of a closed outer carbonate shell. The difference in the measured CO_2 intensity before and after the uptake region in Figure 4 and the integrated area of the traces in Figure 5 are indicators of the amount of CO_2 captured. In all cases, this decreases with each successive capture step. The drop in capacity is most pronounced between the first and second carbonation steps, most notably in the case of the Pure and Co-doped samples.

Figure 6 shows the CO_2 release profiles measured during calcination of the Pure and 2.5 wt.% TM-doped $CaCO_3$ samples in ~0.1 mbar H_2O vapour. “Release 0” corresponds to calcination of the as-prepared $CaCO_3$ samples. These are the same traces that are plotted in Figure 3. “Release 1” to “Release 5” from the various samples follow the “Capture” steps shown in Figure 4. Thus, “Release 1” follows “Capture 1”, and so forth. Since the initial calcination is not entirely effective, a small fraction of the original carbonate remains, which becomes the source of the high-temperature CO_2 peak on some “Release 1” traces, most clearly evident for the Pure and Fe-doped samples. Since “Release 0” corresponds to release from a 100 % carbonate samples, it is clear that none of the recapture steps comes close to fully reloading the samples. This may, in part, be a limitation of the capture procedure employed and does not necessarily reflect the maximum loading that might be achieved under more typical (ambient pressure) carbonation conditions.

Several trends are identifiable in Figure 6. The amount of CO_2 released drops with each successive cycle, consistent with the decreasing uptake that is evident in Figures 4 and 5. Some of the sorbents show a change in the onset of CO_2 release time (temperature). The Pure and Fe-doped samples exhibit better release at lower temperatures compared to the as-prepared sample, while the Ni-doped sample performs worse. Most of the samples exhibit a doublet structure, which tends to become more pronounced with successive cycling. The lower temperature component of the doublet is comparatively stable with repeated cycling. The reduction in CO_2 loading arises primarily from a decrease in the higher temperature component. This feature is also consistent with a model of an easily formed outer carbonate layer and a diffusion-limited bulk.

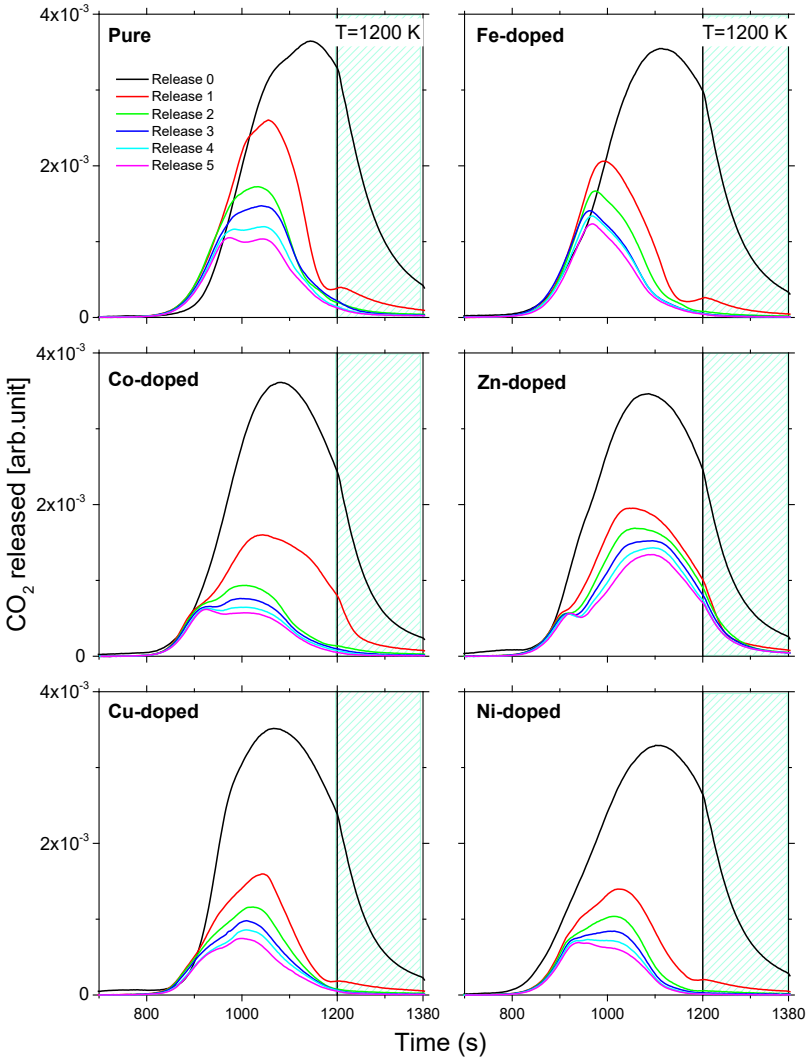

Figure 6: CO_2 release profiles during calcination of Pure and 2.5 wt.% TM-doped $CaCO_3$ in ~0.1 mbar H_2O vapour at 1200 K. The trace legend applies to all panels. The time axes have been shifted such that the time values during the ramping phase (t≤1200 s) are equivalent to the temperature values. The shaded regions indicate the temperature plateau region (T=1200 K).

It is noteworthy that the samples that exhibit rapid uptake in Figures 4 and 5 (Zn-doped during all capture cycles and Co-doped during "Capture 1") also require a longer time (and higher temperature) to subsequently re-release the CO_2. The release traces for these samples extend into the temperature plateau of the thermal cycles. This is consistent with rapid CO_2 capture by these samples being associated with faster uptake by the material bulk. In contrast, the other samples are effectively depleted of recaptured CO_2 before the temperature plateau is attained, suggesting that the carbonate formed is more surface localized.

Figure 7 shows plots of the integrated CO_2 released from the various samples during calcination. All samples show a rapid deterioration in carrying capacity after the initial calcination, followed by a more gradual deterioration during subsequent cycling. Deterioration in capture capacity with cycling is typical of the CaL process and is not an unexpected result. In spite of the very different calcination conditions used in this study, the performance of the Pure sample over the five cycles

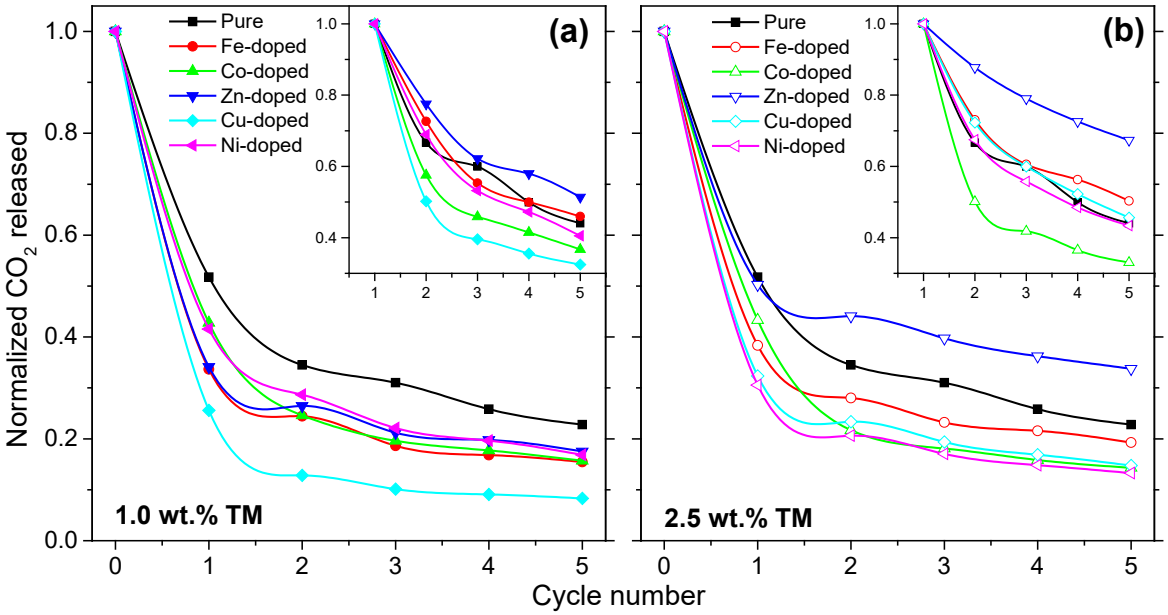

Figure 7: Integrated CO_2 release data for calcination of (a) Pure and 1.0 wt.% TM-doped $CaCO_3$ and (b) Pure and 2.5 wt.% TM-doped $CaCO_3$ in ~0.1 mbar of H_2O vapour. Data points are normalized to the respective "Release 0" values. The insets on the panels show the same data after normalized to the "Release 1" values.

is quite comparable to that reported for $CaCO_3$ samples tested under more application-relevant conditions (see for examples: references [17], [20], [21], [23], and [26]). Although testing over extended cycles has not been done, comparison with these other works suggests that the gradual loss in carrying capacity seen during cycles 2-5 is likely to persist.

Figure 7(a) shows data for calcination of the 1.0 wt.% TM-doped $CaCO_3$ samples while Figure 7(b) shows similar data for the 2.5 wt.% TM-doped samples. The data points on Figure 7(b) are derived from integration of the release traces plotted in Figure 6. In the case of the 2.5 wt.% samples, the Zn-doped sample performs better than Pure $CaCO_3$, whereas all other TM-doped samples perform worse. For the 1.0 wt.% doped samples, all perform worse than Pure $CaCO_3$ with the Cu-doped sample being significantly worse. The insets on Figures 7(a) and (b) show the same datasets but now normalized to the integrated area of the "Release 1" curves. These plots illustrate how well the various samples maintain their initial recapture performance during subsequent recapture cycles. Presented in this fashion, the 2.5 wt.% Zn-doped sample clearly performs best whereas the 2.5 wt.% Co-doped sample appears very poor. The latter is somewhat misleading since rapid uptake by this sample is only exhibited during the first capture cycle, which makes the relative drop in subsequent performance much larger. The main panel shows that the overall performance of the 2.5 wt.% Co-doped sample is comparable to that of Cu and Ni in absolute terms.

b. *Cyclic capture-release in ~0.1 mbar H_2O plasma (100 W)*

Unlike H_2O vapour, calcination under H_2O plasma introduces CO production mechanisms that complicate the evaluation of the CO_2 release profiles. A requirement for the current work is to properly account for the conversion of CO_2 to CO so that cross-comparison of the capture performance of samples calcined under the two different conditions can be made. The

Supplementary Information illustrates the effects of plasma conversion on the measured traces and gives details of the correction procedures that are employed.

The carbonation procedure for samples calcined under H_2O plasma was identical to that used after calcination under H_2O vapour. Figure 8 shows the CO_2 recapture profiles of the various samples following plasma calcination. These traces are directly comparable to those shown in Figure 5 for

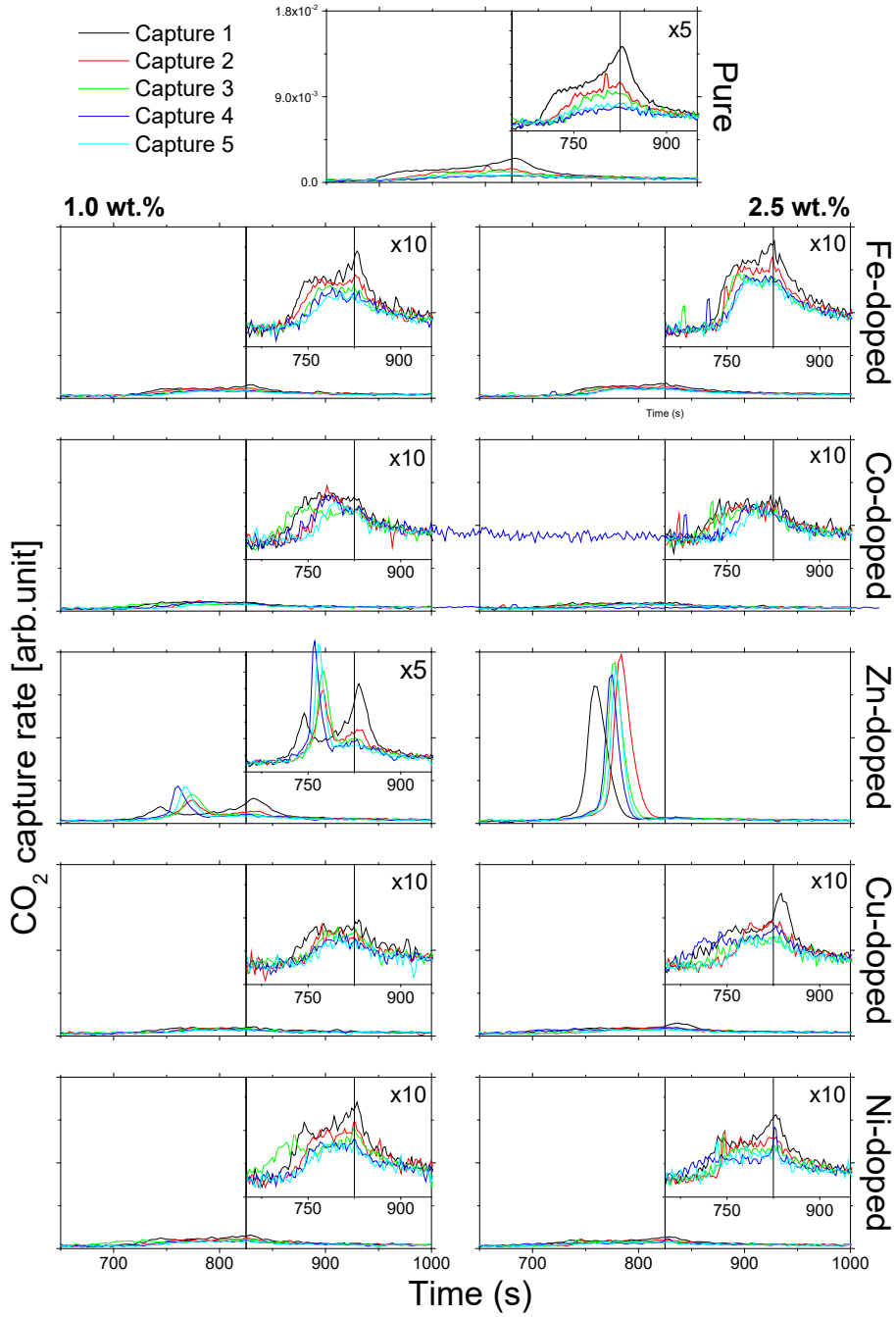

Figure 8: CO_2 recapture rates of Pure (top panel), 1.0 wt.% (left column) and 2.5 wt.% (right column) TM-doped $CaCO_3$ samples after calcination in ~0.1 mbar 100 W H_2O plasma. The trace legend applies to all panels. The insets show expanded views of the main panel data. The vertical lines indicate the transition from the 1 K/s temperature ramp to the T=825 K temperature plateau phase.

recapture after calcination in H_2O vapour. In general, the capture behaviour is similar. The main difference is that rapid uptake of CO_2 during the first recapture cycle of the Co-doped samples is not evident after calcination in plasma. Another clear difference is that the presence of H_2O plasma has a pronounced influence on the recapture characteristics of the 1.0 wt.% Zn sample. A much clearer double peak structure is presented during recapture, which evolves over successive cycles. By the fifth recapture cycle, the uptake profile becomes dominated by the low-temperature peak, which is reminiscent of (though weaker than) the recapture peak exhibited by the 2.5 wt.% Zn sample. In general, with the specific exception of the Zn-doped samples, the TM-doped capture performance appears somewhat worse (lower capture rates) after plasma calcination as compared with the equivalent sample after vapour calcination.

In terms of release performance, the trends observed for calcination under H_2O plasma (not shown) resemble those seen in Figure 6 for calcination under H_2O vapour. The one notable difference was that the release from the 2.5 wt.% Cu-doped sample during cycles 1-5 was delayed with respect to that of "Release 0". In this case, the release profiles more closely resembled those of the Ni-doped sample shown in Figure 6. Figure 9(a) and (b) show the integrated CO_2 release data for decomposition under H_2O plasma, which is directly comparable to the data for H_2O vapour calcination shown in Figure 7. Compared to calcination under H_2O vapour, the performance of the Pure sample is somewhat deteriorated, while that of the 2.5 wt.% Zn-doped sample is slightly improved. The latter now has a higher recapture capacity and still exhibits rapid uptake and good reproducibility over repeated cycles. The overall performance of the other TM-doped samples is not dramatically affected by calcination under H_2O plasma.

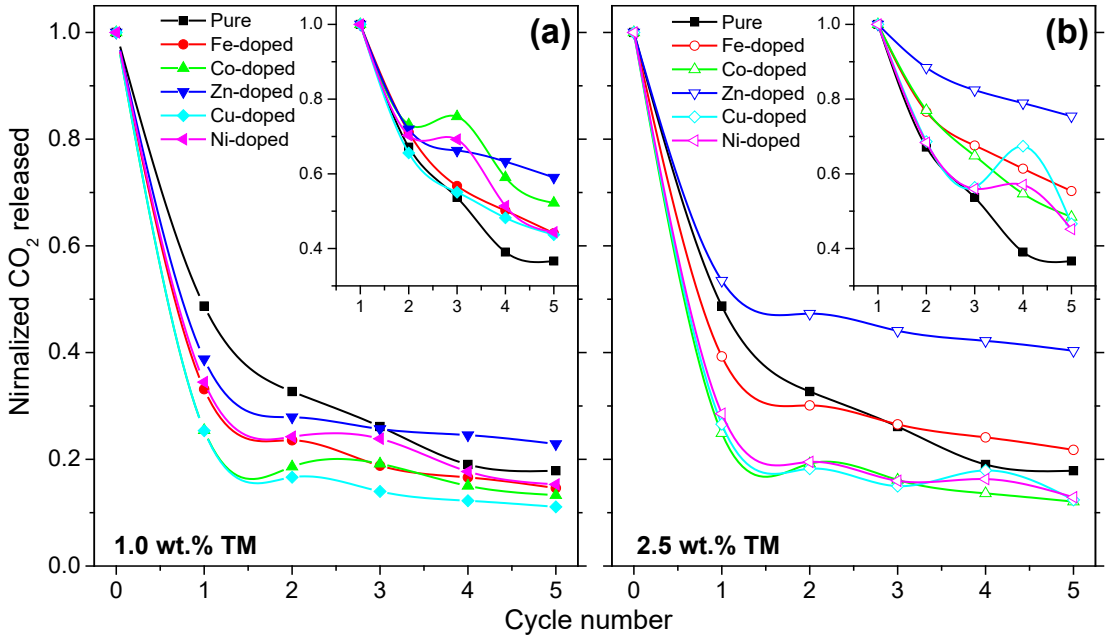

Figure 9: Integrated CO_2 release data for calcination of (a) Pure and 1.0 wt.% TM-doped $CaCO_3$ and (b) Pure and 2.5 wt.% TM-doped $CaCO_3$ in ~0.1 mbar 100W H_2O plasma. Data points are normalized to the respective "Release 0" values. The insets on the panels show the same data after normalized to the "Release 1" values.

When the data is normalized to the integrated area of "Release 1" (insets on Figures 9(a) and (b)), the Pure sample exhibits the worst performance. Directly comparing the trace of the same sorbent for calcination under H_2O vapour and H_2O plasma suggest that the difference in relative performance between the Pure and TM-doped samples when calcined under H_2O plasma is mainly due to a deterioration in the performance of the Pure $CaCO_3$. The presence of TM-doping appears to counteract this effect resulting in more minor changes to the overall performance. Zn-doped samples are notable as the only ones to exhibit a consistent improvement when calcined under H_2O plasma.

c. Comparison of cyclic capture-release of 1.0 wt.%, 2.5 wt.%, and 5.0 wt.% Zinc

In the preceding sections, the Zn-doped samples exhibit the most promising performance for calcination both in H_2O vapour and H_2O plasma. Figure 10 shows a comparison of the CO_2 recapture traces of Zn-doped samples under both conditions, with the addition of data for a 5.0 wt.% Zn-doped samples. When calcined under vapour, the 5.0 wt.% Zn-doped sample shows behaviour similar to that of the 1.0 and 2.5 wt.% Co-doped samples shown in Figure 5. Rapid uptake is observed during the first recapture cycle, but subsequent cycles exhibit much slower recapture. Thus, the beneficial effects of Zn doping are only observed to be persistent within a relatively narrow doping range. When calcined under H_2O plasma, the cyclic performance of the 5.0 wt.% Zn sample is improved relative to the vapour case. The behaviour is qualitatively similar to that

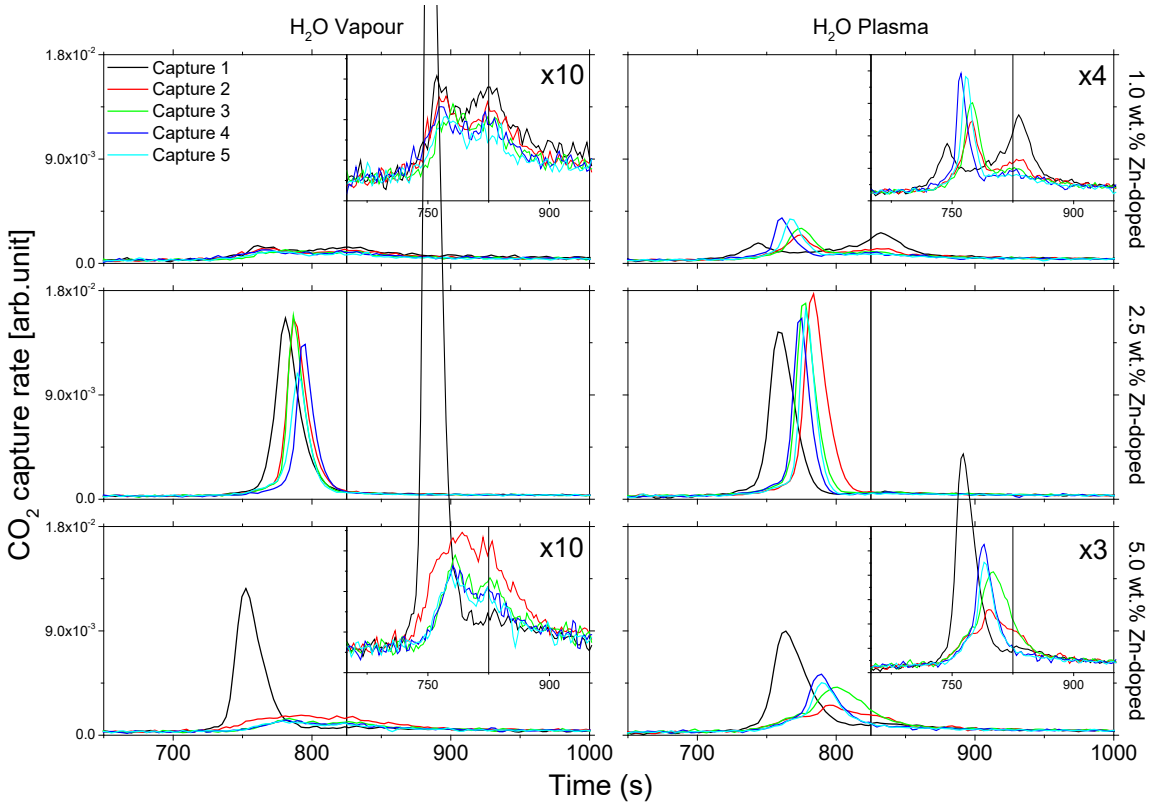

Figure 10: CO_2 capture rate of 1.0, 2.5, and 5.0 wt.% Zn-doped $CaCO_3$ after calcination in H_2O vapour (left column) and H_2O plasma (right column). The trace legend applies to all panels. The insets show expanded views of the main panel data. The vertical lines indicate the transition from the 1 K/s temperature ramp to the T=825 K temperature plateau phase.

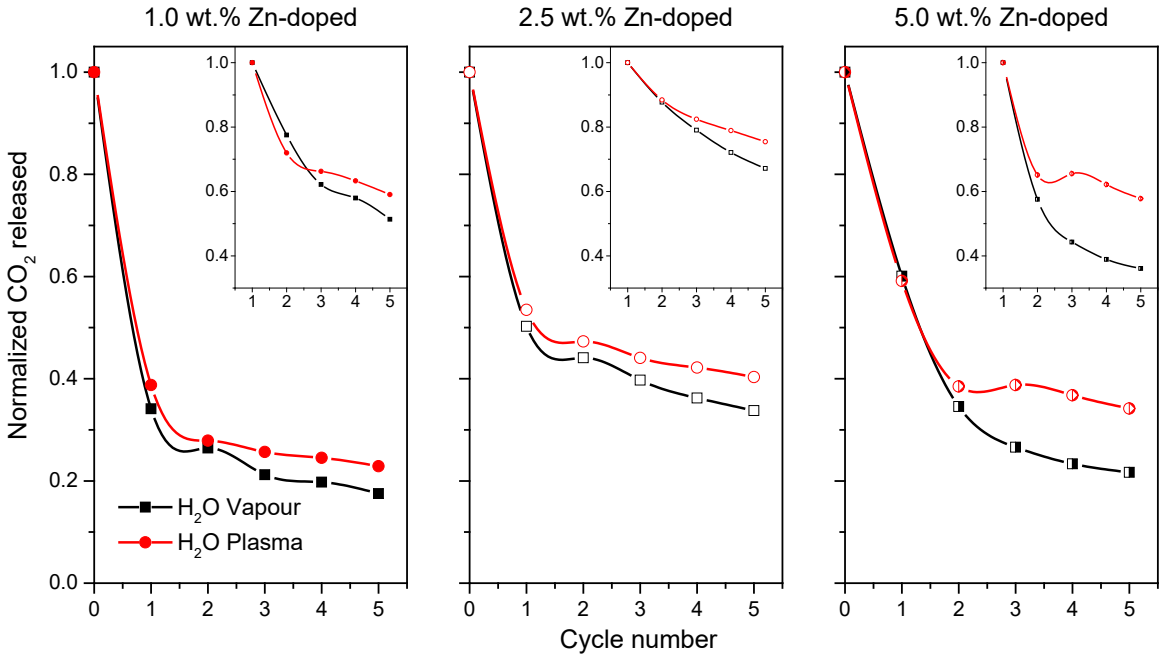

Figure 11: Integrate CO_2 release data from 1.0, 2.5, and 5.0 wt.% Zn-doped samples after calcination in H_2O vapour and H_2O plasma. The traces have been normalized to the "Release 0" values. The insets show the same data after normalization to the "Release 1" values.

exhibited by the 1.0 wt.% Zn-doped sample, with the uptake curve undergoing a progressive development over the repeat cycles and the emergence of a relatively well-defined and rapid uptake profile during "Capture 5".

Comparing the profiles obtained after calcination in vapour and plasma, it is clear that plasma has a discernible influence in all cases. Calcination under plasma increases the subsequent capture rate as compared with calcination under H_2O vapour. For calcination under vapour, successive recaptures typically occur at a similar or slightly higher temperature. In contrast, the effects of plasma calcination on recapture is more complex. In all cases "Capture 2" required a higher temperature than "Capture 1". However, subsequent recaptures occur at somewhat lower temperatures than that of "Capture 2". The influence of plasma on the capture performance evolves continually over the five cycles, as is most evident from the 1.0 wt.% and 5.0 wt.% samples. The gradual evolution may be due to the low pressure in which the plasma is produced. A higher pressure, higher density plasma can be anticipated to have a stronger impact on the material.

Figure 11 illustrates how the integrated CO_2 released from the 1.0 wt.%, 2.5 wt.%, and 5.0 wt.% Zn-doped samples varies during cycling with calcination under H_2O vapour and H_2O plasma. For calcination in vapour, the 2.5 wt.% Zn-doped sample has the best overall performance. The performance of all three samples is improved by calcination in H_2O plasma, with the performance enhancement increasing with increasing Zn content. The carrying capacity of the 5.0 wt.% Zn sample is comparable to that of the 2.5 wt.% sample after plasma calcination, although the recapture performance is not as good (Figure 10).

Tables 3 and 4 provide a tabulation of the fractional release of CO_2 from the various samples during the different release cycles relative to the fully-loaded sample ("Release Cycle 0") for calcination under water vapour and water plasma, respectively. These tables compile the data used to produce the traces show in Figures 7, 9, and 11 for easy cross-comparison.

Table 3: Fraction of CO_2 released during calcination under water vapour relative to the fully-loaded sample ("Release Cycle 0"). This data is the basis for plots shown in Figures 7 and 11.

		Samples calcined in water vapour											
		Pure	Fe-doped		Co-doped		Zn-doped			Cu-doped		Ni-doped	
		0%	1%	2.5%	1%	2.5%	1%	2.5%	5%	1%	2.5%	1%	2.5%
Release Cycle	0	1	1	1	1	1	1	1	1	1	1	1	1
	1	0.52	0.34	0.38	0.43	0.43	0.34	0.50	0.6	0.26	0.32	0.42	0.31
	2	0.35	0.24	0.28	0.25	0.22	0.26	0.44	0.35	0.13	0.23	0.29	0.21
	3	0.31	0.19	0.23	0.20	0.18	0.21	0.40	0.27	0.10	0.19	0.22	0.17
	4	0.26	0.17	0.22	0.18	0.16	0.20	0.36	0.23	0.09	0.17	0.20	0.15
	5	0.23	0.15	0.19	0.16	0.14	0.18	0.34	0.22	0.08	0.15	0.17	0.13

Table 4: Fraction of CO_2 released during calcination under water vapour relative to the fully-loaded sample ("Release Cycle 0"). This data is the basis for plots shown in Figures 9 and 11.

		Samples calcined in water plasma											
		Pure	Fe-doped		Co-doped		Zn-doped			Cu-doped		Ni-doped	
		0%	1%	2.5%	1%	2.5%	1%	2.5%	5%	1%	2.5%	1%	2.5%
Release Cycle	0	1	1	1	1	1	1	1	1	1	1	1	1
	1	0.49	0.33	0.39	0.25	0.25	0.39	0.53	0.59	0.25	0.27	0.34	0.29
	2	0.33	0.24	0.30	0.19	0.19	0.28	0.47	0.39	0.17	0.18	0.24	0.20
	3	0.26	0.19	0.27	0.19	0.16	0.26	0.44	0.39	0.14	0.15	0.24	0.16
	4	0.19	0.17	0.24	0.15	0.14	0.25	0.42	0.37	0.12	0.18	0.18	0.16
	5	0.18	0.15	0.22	0.13	0.12	0.23	0.40	0.34	0.11	0.12	0.15	0.13

d. Characterization of Zn-doped samples

XRD patterns of as-prepared 1.0 wt.%, 2.5 wt.%,and 5.0 wt.% Zn sample are shown in Figure 12(a)-(c). All three samples are a mixture of calcite (the most thermodynamically stable polymorph of $CaCO_3$) and vaterite. Vaterite is the dominant crystal phase in all three samples (see phase % in the figure panels). Vaterite transforms to calcite at ~600-625 K [32].

Figure 12(d) compares XRD patterns measured from the 5.0 wt.% Zn-doped sample after the 5 cycles of capture-release in vapour and plasma. The calcined samples are predominantly CaO. Peaks due to pure ZnO crystalline phase are also evident along with a small fraction of $CaCO_3$. The relative quantities of the three phases are comparable (see Table 5). Quantitative analysis indicates differences in the crystallite sizes of the CaO, ZnO, and $CaCO_3$ phases after calcination in

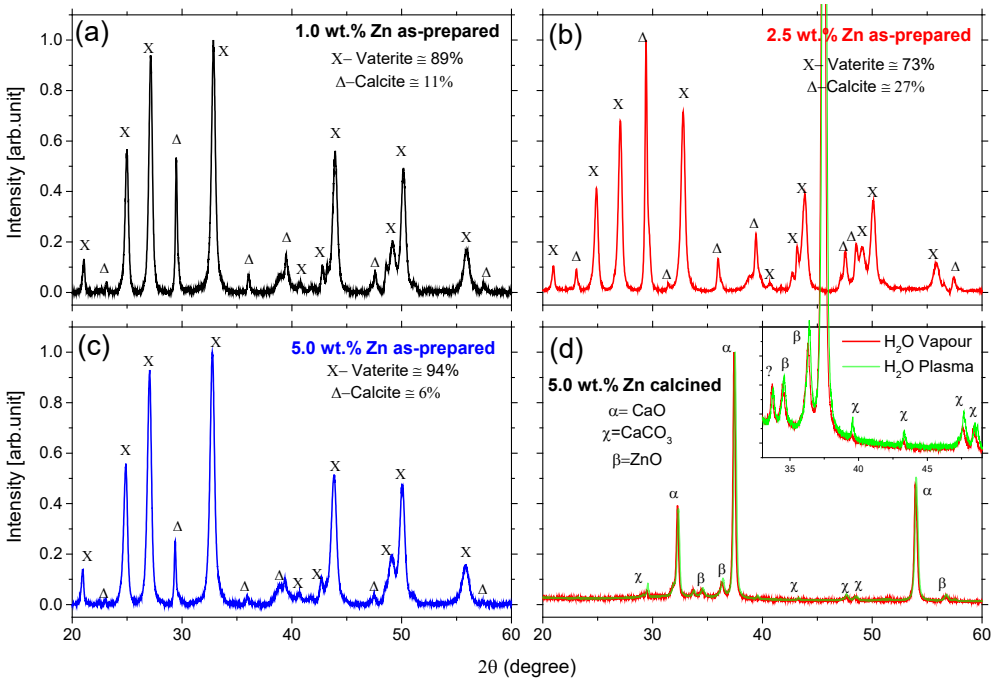

Figure 12: XRD patterns of Zn-doped $CaCO_3$. (a) 1.0 wt.% Zn as-prepared, (b) 2.5 wt.% Zn as-prepared, (c) 5.0 wt.% Zn as-prepared, (d) 5.0 wt.% Zn after calcination (5 cycles) in H_2O vapour and H_2O plasma.

H_2O vapour and H_2O plasma. The crystallite size of the CaO and ZnO phases are somewhat smaller after cycling involved H_2O plasma calcination, while the size of the $CaCO_3$ crystallites is larger.

Figure 13 compares SEM images of Pure, 1.0 wt.% and 2.5 wt.% Zn-doped samples after the five capture/release cycles with calcination in H_2O vapour (left-hand column) and H_2O plasma (right-hand column). Compared to the Pure samples, the Zn-doped samples exhibit less agglomeration and generally smaller and more discrete particles. Comparing the outcome of H_2O vapour and H_2O plasma calcination, there is not a dramatic difference in the case of the Pure samples, although the surface of the plasma-calcined sample appears somewhat more structured and open. A more pronounced effect is apparent from the comparison of the Zn-doped samples. It is most evident in the case of the 1.0 wt.% samples. In light of the comparisons of the uptake rate and the carrying capacity shown in Figures 10 and 11, respectively, it appears that the main impact of plasma-induced material modification is on the CO_2 recapture rate. Although the effect is less pronounced, the carrying capacity is also improved by H_2O plasma calcination.

Table 5: Quantification of crystallite size and quantity of phases formed after calcination (5 cycles) of 5.0 wt. % Zn-doped $CaCO_3$ in H_2O vapour and H_2O plasma.

	Crystallite size (nm)			Quantity (%)		
	CaO	ZnO	$CaCO_3$	CaO	ZnO	$CaCO_3$
Vapour	53.0	46.1	60.0	96.0	3.4	1.1
Plasma	45.6	33.4	68.6	94.4	4.3	1.4

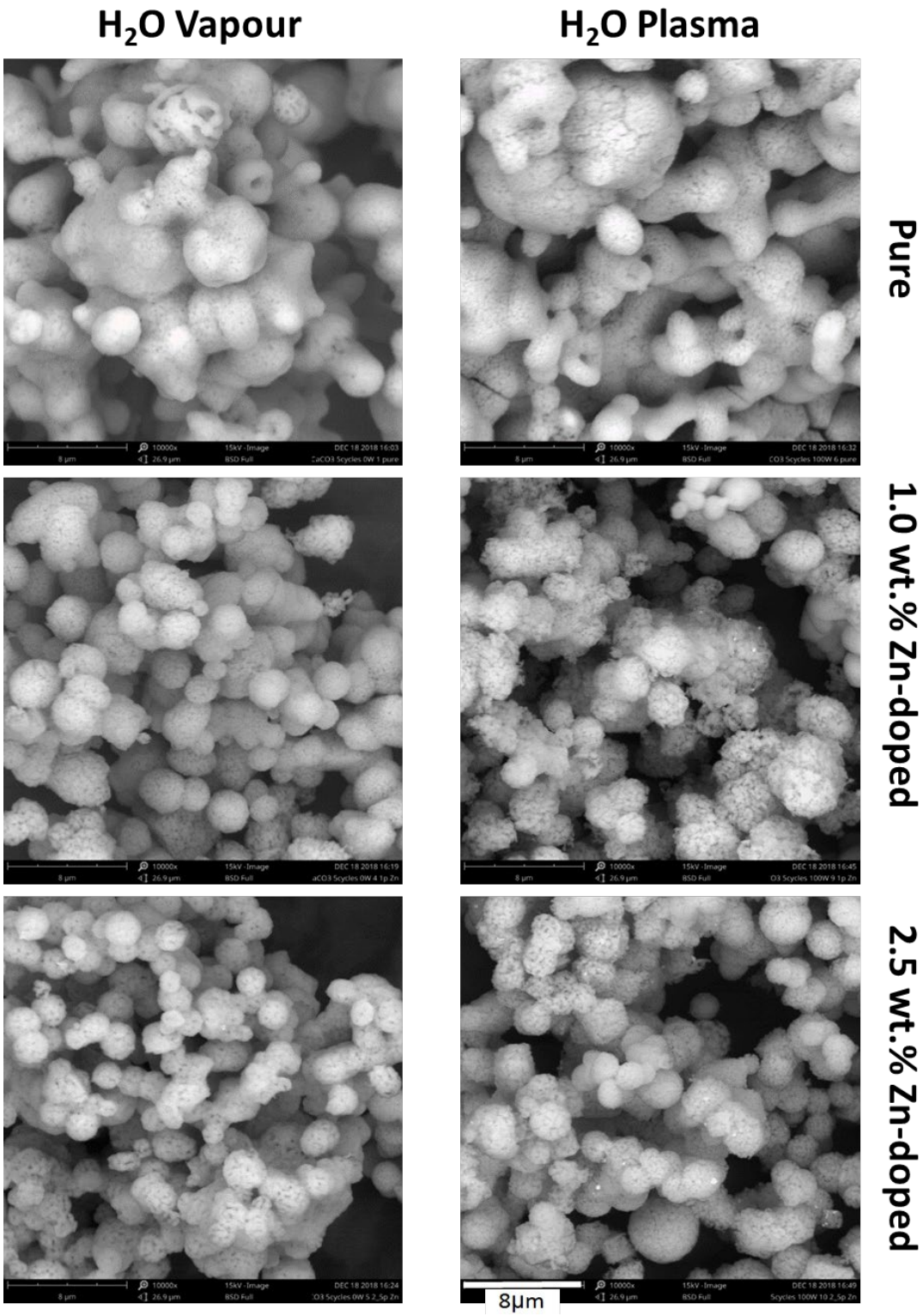

Figure 13: SEM images of (from top to bottom) Pure, 1.0 wt.% Zn-doped and 2.5 wt.% Zn-doped $CaCO_3$ after 5 capture/release cycles with calcination in H_2O vapour (left-hand column) and H_2O plasma (right-hand column). All pictures have the same size and magnification (x10000).

The improved CaL performance induced by Zn-doping under both water vapour and water plasma is an intriguing result. Considering the recapture profiles observed, these samples can be expected to maintain at least the same performance for a somewhat reduced plateau temperature and a much shorter (or zero) plateau time. This would significantly reduce the overall cycling time and contribute to minimizing materials deterioration over multiple cycles. An open question is if the rapid recapture behaviour observed under the current conditions will also manifest for cycling under more application-relevant ambient pressure conditions. On the negative side, the rapid uptake of CO_2 by the Zn-doped samples is coupled to a longer (higher temperature) release profile during subsequent calcination, which is counter-productive in terms of minimizing sample sintering. In contrast, the $CaCO_3$ samples that do not exhibit rapid recapture subsequently released their captured CO_2 at a lower temperature. This suggests that these samples can be calcined under "gentler" conditions. In terms of energy efficiency and long-term material performance, this may, on balance, be a more desirable characteristic than rapid recapture.

It is important to reiterate that the conditions used in the current work are far from those of a realistic process. Consequently it still has to be established if the benefits reported here would also be observed under application conditions. The current work utilizes entirely synthetic calcium carbonates. The synthesis method employed would not be a realistic option for large scale productions since it would remove one of the major advantages of CaL, namely its ready availability in a cheap and abundant natural form. If TM-doped carbonates are to be utilized on a large scale, such as is required for the CaL cycle, then the doped materials should be derived from natural calcium carbonate. This might be feasible using a process based on the well-established Kraft process that is used in paper production. A variant on this process has been proposes for direct capture of CO_2 from air using an NaOH solution to form Na_2CO_3, which is followed by a causticization step where the $Ca(OH)_2$ solution reacts with the Na_2CO_3 to precipitate $CaCO_3$ and regenerate the NaOH [41], [42]. The $CaCO_3$ is then calcined to CaO and subsequently hydrated to regenerated the $Ca(OH)_2$ solution. Modifying this scheme by including TM-doping as part of the causticization step and using a continuous input of natural $CaCO_3$ rather than cycling could provide a means of producing doped $CaCO_3$ that is based on an already well-established industrial process.

Alternatively, it may be an option to incorporate doping as part of existing physical processing of calcium carbonate in order to produce pellets for used in fluidized bed operation and/or into processes used for reactivation of spent sorbent. The latter would be crucial in the event that TM-doped $CaCO_3$ would be susceptible to loss by elutriation during process operation. Various methods of producing CaO-based pellets with enhanced performance and stability are being test (for examples, see [43] and [44]). Incorporating TM doping as part of such steps would potentially be the most economical approach, provided that it results in a performance enhancement comparable to that observed from the chemically-synthesised samples. For sorbent regeneration, methods that utilize water rather than steam (for example [45]) may allow for dopant replenishment via addition to the regenerating solution.

Conclusions

The CaL performance of TM-doped calcium carbonate samples has been evaluated for low-pressure calcination under H_2O vapour and H_2O plasma. The main results of this study are:

- In general, TM doping did not have a persistent impact on the cyclic CaL performance, except in the specific case of Zn doping;
- Zn-doped samples derived from a 2.5 wt.% precursor solution exhibited the best performance, with rapid recapture and better retention of carrying capacity over multiple cycles;
- The performance of the Zn-doped samples was dependent on the wt.% of the precursor solution; samples derived from both 1.0 wt.% and 5.0 wt.% performing worse than the 2.5 wt.% sample;
- The impact of H_2O plasma calcination on the CaL performance was mixed, with some samples exhibiting improvement and others deterioration relative to H_2O vapour calcination;
- The performance of all of the Zn-doped samples improved in the case of H_2O plasma calcination, both in terms of the rate and temperature of CO_2 uptake and in the amount of CO_2 recaptured. The effects were most pronounced in the case of the 1.0 wt.% and 5.0 wt.% samples. The improvement was less dramatic in the case of the 2.5 wt.% sample which already exhibited the best CaL performance during calcination under H_2O vapour.
- Calcination under H_2O plasma results in a more structured, open material morphology.

Plasma calcination most clearly benefited the CaL performance of the Zn-doped samples. It had a discernible effect on the evolution of the material structure. The fact that a significant performance enhancement was not observed for other TM-doped samples suggests a synergistic effect between the plasma interaction and the Zn-doped material rather than a general plasma-materials processing effect is responsible for the observed improvement. While the processing effects of plasma shown in the current study are not dramatic, they are the results of exposure to a low-density plasma. Higher pressure, higher density plasma calcination can be expected to result in more pronounced and rapid material processing.

Acknowledgements

DIFFER is part of the Dutch institutes organisation of NWO. This work is part of the research programme CO2-Neutral Fuels with project number 13CO23-1, which is partly financed by NWO and supported by Shell. The authors thank Erwin Zoethout for performing the SEM measurements.

References

[1] Global CCS Institute, "The global status of CCS report" Melbourne, Australia, https://www.globalccsinstitute.com/resources/global-status-report/.
[2] S. Vijayavenkataraman, S. Iniyan, and R. Goic, "A review of climate change, mitigation and adaptation" *Renew. Sustain. Energy Rev.*, vol. 16, no. 1, pp. 878–897, 2012.
[3] M. E. Boot-Handford *et al.*, "Carbon capture and storage update" *Energy Environ. Sci.*, vol. 7, no. 1, pp. 130–189, 2014.
[4] H. Dieter, C. Hawthorne, M. Zieba, and G. Scheffknecht, "Progress in calcium looping post combustion CO_2 capture: Successful pilot scale demonstration" *Energy Procedia*, vol. 37, pp. 48–56, 2013.
[5] M. Broda, R. Pacciani, and Christoph R. Müller, "CO_2 capture via cyclic calcination and carbonation reactions" in *Porous materials for carbon dioxide capture*, A.-H. Lu and S. Dai, Eds. Heidelberg: Springer, 2013, pp. 181–222.
[6] W. F. L. M. Hoeben, E. J. M. Van Heesch, F. J. C. M. Beckers, W. Boekhoven, and A. J. M. Pemen, "Plasma driven, water assisted CO_2 methanation" *IEEE Xplore*, vol. 43, no. 6, pp. 1–6, 2015.
[7] S. Mahammadunnisa, E. L. Reddy, D. Ray, C. Subrahmanyam, and J. C. Whitehead, "CO_2 reduction to syngas and carbon nanofibres by plasma-assisted in situ decomposition of water" *Int. J. Greenh. Gas Control*, vol. 16, no. 1, pp. 361–363, 2013.
[8] M. Kraus, W. Egli, K. Haffner, B. Eliasson, U. Kogelschatz, and A. Wokaun, "Investigation of mechanistic aspects of the catalytic CO_2 reforming of methane in a dielectric-barrier discharge using optical emission spectroscopy and kinetic modeling" *Phys. Chem. Chem. Phys.*, vol. 4, no. 4, pp. 668–675, 2002.
[9] M. Werner, S. Hariharan, and M. Mazzotti, "Flue gas CO_2 mineralization using thermally activated serpentine: From single- to double-step carbonation" *Energy Procedia*, vol. 63, pp. 5912–5917, 2014.
[10] A. Sanna, M. Uibu, G. Caramanna, R. Kuusik, and M. M. Maroto-Valer, "A review of mineral carbonation technologies to sequester CO_2" *Chem. Soc. Rev.*, vol. 43, no. 23, pp. 8049–8080, 2014.
[11] D. Y. C. Leung, G. Caramanna, and M. M. Maroto-Valer, "An overview of current status of carbon dioxide capture and storage technologies" *Renew. Sustain. Energy Rev.*, vol. 39, pp. 426–443, 2014.
[12] C. C. Dean, J. Blamey, N. H. Florin, M. J. Al-Jeboori, and P. S. Fennell, "The calcium looping cycle for CO_2 capture from power generation, cement manufacture and hydrogen production" *Chem. Eng. Res. Des.*, vol. 89, no. 6, pp. 836–855, 2011.
[13] D. Beruto, "Thermodynamics and kinetics of carbon dioxide chemisorption on calcium oxide" *J. Phys. Chem.*, vol. 88, no. 18, pp. 4052–4055, 1984.
[14] M. E. Diego *et al.*, "Calcium looping with enhanced sorbent performance: Experimental testing in a large pilot plant" *Energy Procedia*, vol. 63, pp. 2060–2069, 2014.
[15] M. C. Romano *et al.*, "The calcium looping process for low CO_2 emission cement plants" *Energy Procedia*, vol. 61, pp. 500–503, 2014.
[16] M. Erans, M. Jeremias, V. Manovic, and E. J. Anthony, "Operation of a 25 KW_{th} calcium ooping pilot-plant with high oxygen concentrations in the calciner" *J. Vis. Exp.*, no. 128, pp. 1–10, 2017.
[17] J. Blamey, E. J. Anthony, J. Wang, and P. S. Fennell, "The calcium looping cycle for large-scale CO_2 capture" *Prog. Energy Combust. Sci.*, vol. 36, no. 2, pp. 260–279, 2010.
[18] R. H. Borgwardt, "Calcium oxide sintering in atmospheres containing water and carbon dioxide" *Ind. Eng. Chem. Res.*, vol. 28, no. 4, pp. 493–500, 1989.
[19] V. Manovic and E. J. Anthony, "Steam reactivation of spent CaO based sorbent for multiple CO_2 capture cycles" *Environ. Sci. Technol*, vol. 41, no. 4, p. 1420, 2007.
[20] V. Manovic and E. J. Anthony, "Thermal activation of CaO-based sorbent and self-reactivation during CO_2 capture looping cycles" *Environ. Sci. Technol.*, vol. 42, no. 11, pp. 4170–4174, 2008.
[21] V. Manovic, E. J. Anthony, G. Grasa, and J. C. Abanades, "CO_2 looping cycle performance of a high-purity limestone after thermal activation/doping" *Energy and Fuels*, vol. 22, no. 5, pp. 3258–3264, 2008.
[22] H. Pawlak-Kruczek and M. Baranowski, "Effectiveness of CO_2 capture by calcium looping with regenerated calcium sorbents - last step calcination" *Energy Procedia*, vol. 105, pp. 4499–4512, 2017.
[23] P. Sun, J. R. Grace, C. J. Lim, and E. J. Anthony, "Investigation of attempts to improve cyclic CO_2 capture by sorbent hydration and modification" *Ind. Eng. Chem. Res.*, vol. 47, no. 6, pp. 2024–2032, 2008.
[24] B. González *et al.*, "Calcium looping for CO_2 capture: Sorbent enhancement through doping" *Energy Procedia*, vol. 4, pp. 402–409, 2011.
[25] V. Manovic and E. J. Anthony, "Sequential SO_2/CO_2 capture enhanced by steam reactivation of a CaO-based sorbent" *Fuel*, vol. 87, no. 8–9, pp. 1564–1573, 2008.
[26] F. Donat, N. H. Florin, E. J. Anthony, and P. S. Fennell, "Influence of high-temperature steam on the reactivity of CaO sorbent for CO_2 capture" *Environ. Sci. Technol.*, vol. 46, no. 2, pp. 1262–1269, 2012.

[27] R. W. Hughes, D. Lu, E. J. Anthony, and Y. Wu, "Improved long-term conversion of limestone-derived sorbents for in situ capture of CO_2 in a fluidized bed combustor" *Ind. Eng. Chem. Res.*, vol. 43, no. 18, pp. 5529–5539, 2004.
[28] J. Blamey, "Improved performance of CaO-based sorbent for CO_2 capture", PhD thesis, Imperial College London, 2012.
[29] H. Lu, A. Khan, S. E. Pratsinis, and P. G. Smirniotis, "Flame-made durable doped-CaO nanosorbents for CO_2 capture" *Energy & Fuels*, vol. 23, no. 2, pp. 1093–1100, 2009.
[30] R. Koirala, G. K. Reddy, and P. G. Smirniotis, "Single nozzle flame-made highly durable metal doped ca-based sorbents for CO_2 capture at high temperature" *Energy and Fuels*, vol. 26, no. 5, pp. 3103–3109, 2012.
[31] C. Salvador, D. Lu, E. J. Anthony, and J. C. Abanades, "Enhancement of CaO for CO_2 capture in an FBC environment" *Chem. Eng. J.*, vol. 96, no. 1–3, pp. 187–195, 2003.
[32] T. T. Belete, M. C. M. van de Sanden, and M. A. Gleeson, "Effects of transition metal dopants on the calcination of $CaCO_3$ under Ar, H_2O and H_2" *J. CO_2 Util.*, vol. 31, no. February, pp. 152–166, 2019.
[33] Y. Wang and W. J. Thomson, "The effects of steam and carbon dioxide on calcite decomposition using dynamic X-ray-diffraction" *Chem. Eng. Sci.*, vol. 50, no. 9, pp. 1373–1382, 1995.
[34] V. L. Boris, "Mechanism of thermal decomposition of alkaline-earth carbonates" *Thermochim. Acta*, vol. 303, pp. 161–170, 1997.
[35] C. Padeste, A. Reller, and H. R. Oswald, "The influence of transition metals on the thermal decomposition of calcium carbonate in hydrogen" *Mater. Res. Bull.*, vol. 25, pp. 1299–1305, 1990.
[36] A. Reller, C. Padeste, and P. Hug, "Formation of organic carbon compounds from metal carbonates" *Nature*, vol. 329, no. 8, pp. 527–529, 1987.
[37] K. Zeppenfeld, "Prevention of $CaCO_3$ scale formation by trace amounts of copper (II) in comparison to zinc (II)" *Desalination*, vol. 252, no. 1–3, pp. 60–65, 2010.
[38] J. Rodríguez-Carvajal, "Recent advances in magnetic structure determination by neutron powder diffraction" *Phys. B Phys. Condens. Matter*, vol. 192, no. 1–2, pp. 55–69, 1993.
[39] B. Arias, J. C. Abanades, and G. S. Grasa, "An analysis of the effect of carbonation conditions on CaO deactivation curves" *Chem. Eng. J.*, vol. 167, no. 1, pp. 255–261, 2011.
[40] V. Manovic and E. J. Anthony, "Carbonation of CaO-based sorbents enhanced by steam addition" *Ind. Eng. Chem. Res.*, vol. 49, no. 19, pp. 9105–9110, 2010.
[41] American Physical Society, "Direct air capture of CO_2 with chemicals: A technology assessment for the APS Panel on Public Affairs", June 1, 2011.
[42] E. S. Sanz-Pérez, C. R. Murdock, S. A. Didas, and C. W. Jones, "Direct capture of CO_2 from ambient air", *Chem. Rev.*, vol. 116, pp. 11840−11876, 2016.
[43] C. Qin, J. Yin, H. An, W. Liu, and B. Feng, "Performance of extruded particles from calcium hydroxide and cement for CO_2 capture" *Energy and Fuels*, vol. 26, no. 1, pp. 154–161, 2012.
[44] J. Sun, C. Liang, X. Tong, Y. Guo, W. Li, C. Zhao, J. Zhang, and P. Lu, "Evaluation of high-temperature CO_2 capture performance of cellulose-templated CaO-based pellets" *Fuel*, vol. 239, pp. 1046–1054, 2019.
[45] V. Manovic, Y. Wu, I. He, and E. J. Anthony, "Spray water reactivation/pelletization of spent CaO-based sorbent from calcium looping cycles" *Environ. Sci. Technol*., vol. 46, no. 22, pp. 12720-12725, 2012.